Journal of ELECTRONIC MATERIALS, Vol. 39, No. 11, 2010
DOI: 10.1007/s11664-010-1338-6

Elastic Moduli of $(Ni,Cu)_3Sn_4$ Ternary Alloys from First-Principles Calculations

FENG GAO[1,3] and JIANMIN QU[1,2]

1.—Department of Civil and Environmental Engineering, Northwestern University, Evanston, IL 60208, USA. 2.—Department of Mechanical Engineering, Northwestern University, Evanston, IL 60208, USA. 3.—e-mail: feng-gao@northwestern.edu

Based on first-principles calculations, the effect of Cu solubility on the elastic moduli of Ni_3Sn_4-based intermetallic compound (IMC) is investigated. It is found that the stiffness tensor of a $(Ni,Cu)_3Sn_4$ single crystal is anisotropic, and the presence of Cu in the crystal compound reduces the moduli of $(Ni,Cu)_3Sn_4$ due to reduced hybridization between Ni and Sn states. Furthermore, our results show that higher Cu concentration in the $(Ni,Cu)_3Sn_4$-based IMCs leads to thermodynamically less stable compounds. Based on the single-crystal results, the elastic properties of polycrystalline $(Ni,Cu)_3Sn_4$ are also obtained.

Key words: Lead-free solder, intermetallic compound, first principles, density of states, single crystal, elastic property

INTRODUCTION

Ni-based finishes, e.g., electroless nickel immersion gold (ENIG), are widely used in electronic packaging. The Ni_3Sn_4 intermetallic compound (IMC) is often found at the interface between Sn-based lead-free solders and ENIG.[1–4] The thermomechanical behavior of such IMCs often plays an important role in determining the failure of solder/pad interfaces; for example, it is well known that excessive IMC growth at the interface can compromise the reliability of solder joints, because IMCs are typically stiffer and brittle. With the ever-increasing demands for miniaturization of electronic devices, the size of solder joints is being reduced dramatically. This reduced solder volume increases the IMC volume fraction of the total volume of the solder joint, making the interfacial behavior more prominent. Recent adoption of lead-free solders further aggravates the influence of interfacial IMCs.

Therefore, it is crucial to know IMCs' thermomechanical properties in order to evaluate solder joint reliability in electronic packaging. One of the most important thermomechanical properties of IMCs is their elastic stiffness. However, existing data on Ni_3Sn_4 elastic constants seem to vary over a wide range; for instance, the reported Young's moduli are between 134 GPa and 158 GPa when measured using nanoindentation, and between 94 GPa and 118 GPa when measured using other methods.[5–9]

Sn-Ag-Cu ternary lead-free solders have been accepted as some of the best candidates for replacement of conventional Sn-Pb solders in electronic packaging. It has been observed that traces of Cu are often present in the Ni_3Sn_4 IMC, where the Cu atoms substitute for the Ni sublattice. Such Ni_3Sn_4-based IMC is usually labeled $(Ni,Cu)_3Sn_4$.[1–4] It is plausible that the presence of Cu may alter the elastic stiffness of this IMC. The focus of the present work is to investigate this effect using a density-functional theory approach. Although, several recent studies have been performed to calculate the elastic properties of binary IMCs that are commonly formed in the solder joint, such as Cu_6Sn_5, Ni_3Sn_4, Ag_3Sn, Cu_3Sn, etc.,[10–12] very few works have studied Ni-Cu-Sn ternary IMCs.

Ni_3Sn_4-BASED MODEL AND SIMULATION METHOD

The Ni_3Sn_4 IMC has a monoclinic crystal structure (space group $C2/m$).[13] Figure 1a depicts the crystal structure of Ni_3Sn_4, in which the Ni atoms

(Received March 22, 2010; accepted July 27, 2010; published online August 14, 2010)

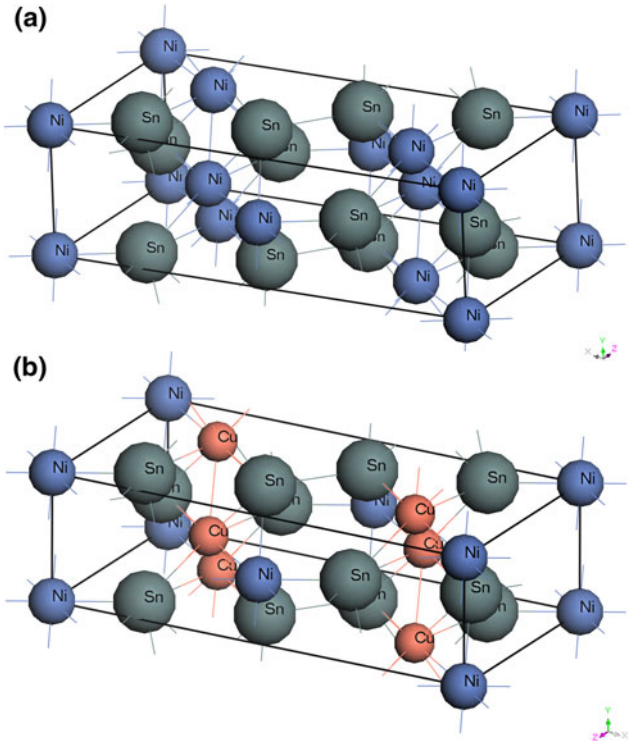

Fig. 1. (a) Unit cell of Ni_3Sn_4; the small blue spheres represent the Ni atoms and the large green spheres represent the Sn atoms. (b) The $Ni_1Cu_2Sn_4$ phase, in which the 4*i* Ni atoms are replaced by Cu atoms.

occupy the 2*a* and 4*i* space sites and the Sn atoms are located at two different 4*i* positions. It has been shown that, in $(Ni,Cu)_3Sn_4$, the Cu atoms substitute for the Ni sublattice and do not change the basic crystal structure of Ni_3Sn_4.[1] Therefore, in this study, the Ni atoms at the 2*a* site are replaced by Cu atoms according to the formula $Ni_2Cu_1Sn_4$, which yields a Cu concentration of 14.3 at.%. Similarly, the formula $Ni_1Cu_2Sn_4$ represents the crystal structure in which the Cu atoms substitute for Ni atoms at the 4*i* site, as shown in Fig. 1b, which yields a Cu concentration of 28.6 at.%.

First-principles calculations were performed using CASTEP software.[14,15] The software uses the plane-wave pseudopotential method and performs energy minimization by the Broyden–Fletcher–Goldfarb–Shanno method. The Perdew–Burke–Ernzerhof (PBE) generalized gradient approximation (GGA) functional was employed to deal with the exchange correlation. The pseudo-atomic calculation was conducted for the following electron configurations: $3d^8 4s^2$ of Ni, $3d^{10} 4s^1$ of Cu, and $5s^2 5p^2$ of Sn. The original lattice constants used as input for the geometry optimization were a = 12.214 Å, b = 4.060 Å, c = 5.219 Å, and β = 105.0°.[13] The energy of the Ni_3Sn_4-based crystal structure was minimized with respect to the lattice constants and any interior degree of freedom. Convergence was considered to be achieved when the following conditions were met simultaneously: energy change below 5×10^{-6} eV/atom, force less than 0.01 eV/Å, stress less than 0.02 GPa, and displacement change less than 5×10^{-4} Å. The energy cutoff was set as 330 eV, and the *k*-point set was $7 \times 7 \times 5$.

Table I. *Ab initio* calculated lattice parameters of $(Ni,Cu)_3Sn_4$ ternary crystals

IMCs	Lattice Parameters (Å) by GGA-PBE
Ni_3Sn_4	a = 12.34460, b = 4.11096, c = 5.32335, β = 105.495 experiment[13]: a = 12.2146, b = 4.0602, c = 5.2913, β = 105.010
$Ni_2Cu_1Sn_4$ (Cu at 2*a* site)	a = 12.42553, b = 4.22212, c = 5.31220, β = 105.977
$Ni_1Cu_2Sn_4$ (Cu at 4*i* site)	a = 12.55115, b = 4.19994, c = 5.44223, β = 106.102

To calculate the elastic constants, the optimized $(Ni,Cu)_3Sn_4$ unit cell was subjected to deformation with various states of strain, in the same manner as used in Karki et al.[16] Specifically, the nonzero strain components used for the four states of strain were, respectively, (i) ε_{11} and ε_{23}, (ii) ε_{33} and ε_{12}, (iii) ε_{22}, and (iv) ε_{13}. In each strain state, the magnitude of these nonzero strain components was gradually increased from 0 to 0.003. For each strain increment, the energy of the unit cell was minimized with the cell vectors fixed, and the corresponding stresses were obtained. The elastic constants were then extracted from a liner fit with the strain increment. Table I shows the lattice parameters obtained from the *ab initio* calculations. It can be seen that the lattice parameters for Ni_3Sn_4 calculated using GGA agree very well with the ambient-temperature experimental data.[13]

Comparing with the lattice parameters of the pure Ni_3Sn_4 crystal structure, we found that the presence of Cu increases the volume of the Ni_3Sn_4 base structure. This may be an indication that Cu occupancy in Ni_3Sn_4 reduces the binding inside the Ni_3Sn_4 crystal structure. To study thermodynamic stability, the total energy of the $(Ni,Cu)_3Sn_4$ crystal was first computed. This total energy was then used to calculate the heat of formation to determine the thermodynamic stability. The heat of formation is related to the composition-average energies of the pure component elements in their equilibrium crystal structure.[17] Therefore, for the formula $Ni_mCu_nSn_k$, the heat of formation at zero Kelvin is given by:

$$\Delta E = \frac{1}{m+n+k}\left[E^{\text{total}}_{Ni_mCu_nSn_k} - (mE_{Ni} + nE_{Cu} + kE_{Sn})\right], \quad (1)$$

where ΔE is the heat of formation, $E^{\text{total}}_{Ni_mCu_nSn_k}$ is the total energy of $Ni_mCu_nSn_k$, E_{Ni}, and E_{Cu}, and E_{Sn} are the energies of the elements Ni, Cu, and Sn,

Table II. Heat of formation of $(Ni,Cu)_3Sn_4$ ternary crystals

IMCs	Heat of Formation (eV/atom)
Ni_3Sn_4	−0.316
$Ni_2Cu_1Sn_4$ (Cu at 2*a* site)	−0.237
$Ni_1Cu_2Sn_4$ (Cu at 4*i* site)	−0.180

respectively. In this study, Ni and Cu have the face-centered cubic structure, and Sn is taken as having the β-Sn crystal structure. The computed heat of formation of the different $(Ni,Cu)_3Sn_4$ phases is presented in Table II. Based on our results, the heat of formation of Ni_3Sn_4 itself is −0.316 eV/atom (about −30.49 kJ/mol). This is comparable to previously reported values of −28.16 kJ/mol (by local density approximation), −23.28 kJ/mol (GGA)[18] −34.26 kJ/mol,[19] and −25.41 kJ/mol[20] (by calculation of phase diagram, CALPHAD), as well as the reported experimental results of −29.68 kJ/mol[21] and −28.76 kJ/mol,[22] both at 298 K. This partially validates our implementation of the first-principles calculations.

It is seen from Table II that all the values of heat of formation are negative. However, Ni_3Sn_4 has the highest absolute value (or lowest heat of formation) among the three phases considered, indicating that the Ni_3Sn_4 crystal structure is more thermodynamically stable. Furthermore, $Ni_1Cu_2Sn_4$ has a higher heat of formation than $Ni_2Cu_1Sn_4$, indicating that the higher Cu concentration in $(Ni,Cu)_3Sn_4$ leads to a higher heat of formation. Since the Cu concentration in $Ni_2Cu_1Sn_4$ is 14.3 at.%, it can be concluded that the Cu solubility in the $(Ni,Cu)_3Sn_4$ phase should not exceed 14.3 at.%. In fact, it has been found that usually the maximum Cu solubility in $(Ni,Cu)_3Sn_4$ is approximately 7.0 at.% to 8.0 at.%,[1–3,23] although a $(Ni,Cu)_3Sn_4$ phase with a slightly higher Cu concentration (10.6 at.%) has also been reported.[3]

The elastic properties of the three phases, Ni_3Sn_4, $Ni_2Cu_1Sn_4$, and $Ni_1Cu_2Sn_4$, were all calculated by using the first-principles approach. Figure 2 illustrates the computed stiffness matrix of single-crystal $(Ni,Cu)_3Sn_4$. It is seen that, in all three phases, c_{33} is greater than c_{11} and c_{22}, indicating elastic anisotropy. Furthermore, c_{11}, c_{22}, and c_{33} of Ni_3Sn_4 are all greater than those of $Ni_2Cu_1Sn_4$ and $Ni_1Cu_2Sn_4$, indicating a higher binding force in Ni_3Sn_4 than in $(Ni,Cu)_3Sn_4$. This is consistent with the calculated results of heat of formation, as shown in Table II.

The calculated single-crystal elastic constants in Fig. 2 cannot be validated directly, as there are no experimental results for comparison. To validate the calculated results, corresponding polycrystalline elastic moduli were computed based on the Voight–Reuss–Hill (VRH) approach.[24] The results are presented in Table III. It is seen that the results in

$$\begin{bmatrix} 155.0 & 70.2 & 66.4 & 0.0 & -21.1 & 0.0 \\ & 155.7 & 71.8 & 0.0 & 9.9 & 0.0 \\ & & 180.1 & 0.0 & -8.6 & 0.0 \\ & & & 57.6 & 0.0 & 9.9 \\ & & & & 59.9 & 55.8 \\ & & & & & 55.8 \end{bmatrix}$$

(a)

$$\begin{bmatrix} 136.5 & 57.6 & 57.7 & 0.0 & -21.9 & 0.0 \\ & 140.5 & 65.2 & 0.0 & 11.6 & 0.0 \\ & & 162.3 & 0.0 & -4.2 & 0.0 \\ & & & 51.7 & 0.0 & 8.9 \\ & & & & 48.2 & 0.0 \\ & & & & & 47.8 \end{bmatrix}$$

(b)

$$\begin{bmatrix} 128.5 & 52.9 & 54.6 & 0.0 & -18.8 & 0.0 \\ & 136.2 & 65.7 & 0.0 & 9.0 & 0.0 \\ & & 141.1 & 0.0 & -2.2 & 0.0 \\ & & & 41.7 & 0.0 & 7.3 \\ & & & & 44.1 & 0.0 \\ & & & & & 46.4 \end{bmatrix}$$

(c)

Fig. 2. Stiffness matrix of single-crystal IMCs: (a) Ni_3Sn_4, (b) $Ni_2Cu_1Sn_4$, and (c) $Ni_1Cu_2Sn_4$.

Table III for Ni_3Sn_4 are consistent with the values measured by nanoindentation.[5–8] For the $(Ni,Cu)_3Sn_4$ phases, the Young's modulus measured by nanoindentation is 164.9 GPa.[25] This is quite different from our calculated result. This difference may be attributed to the thin $(Ni,Cu)_3Sn_4$ layer used for the nanoindentation test. In addition, the lower Cu concentration in $(Ni,Cu)_3Sn_4$ may also be a factor. The results in Table III show that Ni_3Sn_4 has larger elastic moduli than those of $Ni_2Cu_1Sn_4$ and $Ni_1Cu_2Sn_4$.

To understand the binding mechanism in the $(Ni,Cu)_3Sn_4$ crystal structure, electronic structures, such as density of states (DOS) and partial DOS (PDOS), were investigated. The DOS describes the number of states that are available to be occupied at a given energy level, while the PDOS measures the partial contributions from the component elements in the system. Figure 3 shows the total DOS of Ni_3Sn_4, and the PDOS of Ni and Sn atoms. It can be seen that the DOS at the energy range between 0 eV and −3 eV is governed by the Ni *d* state. When the energy is less than −5.5 eV, the Sn *s* state is the dominant part of the DOS, while the Sn *p* state becomes the dominant part of the DOS when the energy is larger than 0 eV. Furthermore, it is clear that hybridization between Ni *d* and Sn *p* at the energy range between −2 eV and −3 eV is the dominant factor of binding in Ni_3Sn_4, consistent with the study by Ghosh.[18]

Table III. Elastic properties of polycrystalline moduli calculated from single-crystal elastic constants

	Bulk Modulus *B* (GPa)	Shear Modulus *G* (GPa)	Young's Modulus *E* (GPa)	Poisson Ratio *v*
Ni_3Sn_4	VRH upper: 100.83	VRH upper: 53.51	VRH upper: 136.40	VRH upper: 0.27
	VRH lower: 99.56	VRH lower: 49.73	VRH lower: 127.90	VRH lower: 0.29
$Ni_2Cu_1Sn_4$	VRH upper: 88.9	VRH upper: 46.8	VRH upper: 119.44	VRH upper: 0.28
	VRH lower: 87.5	VRH lower: 42.7	VRH lower: 110.18	VRH lower 0.29
$Ni_1Cu_2Sn_4$	VRH upper: 83.6	VRH upper: 41.9	VRH upper: 107.71	VRH upper: 0.29
	VRH lower: 82.4	VRH lower: 39.1	VRH lower: 101.28	VRH lower: 0.30

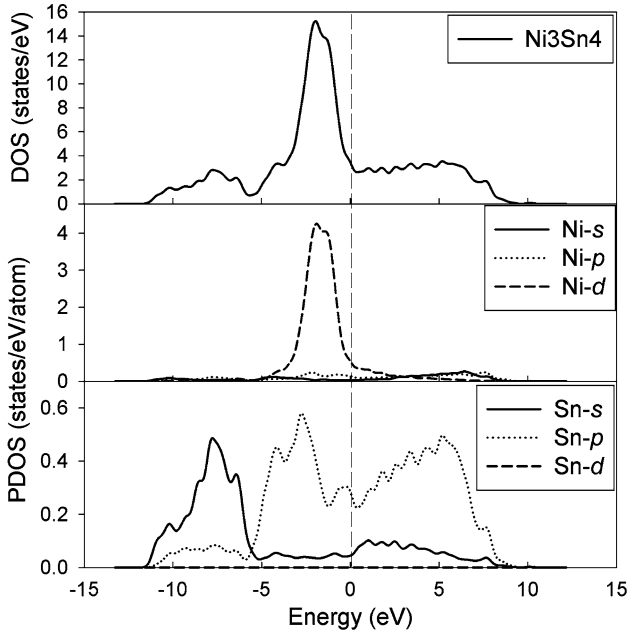

Fig. 3. Total DOS of Ni_3Sn_4 and PDOS of Ni and Sn atoms.

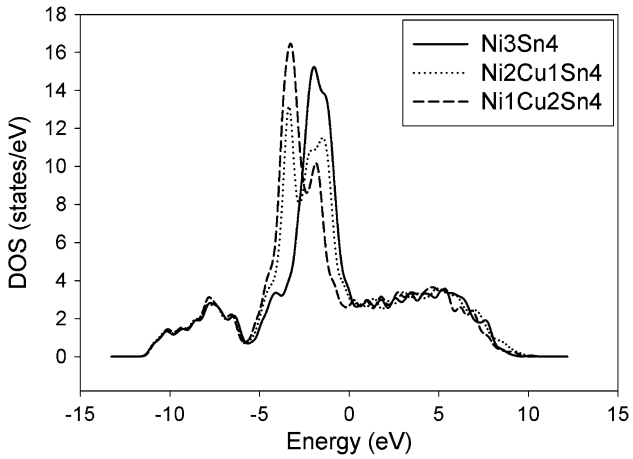

Fig. 4. Total DOS comparison among Ni_3Sn_4, $Ni_2Cu_1Sn_4$, and $Ni_1Cu_2Sn_4$.

When Cu atoms substitute for Ni atoms in the Ni_3Sn_4 crystal structure, the DOS and PDOS profiles are altered significantly. A second peak appears near the Ni *d* state peak position, which may be mainly contributed by the Cu atom states, as shown in Fig. 4. The resulting PDOS of Ni, Cu, and Sn atoms in $Ni_2Cu_1Sn_4$ are illustrated in Fig. 5. It can be seen that hybridization between Ni *d* and Sn *p* states at the energy range −2.0 eV to −2.5 eV is still dominant in the binding in $Ni_2Cu_1Sn_4$. However, the amplitude of the Ni *d* state peak is significantly reduced due to the low Ni concentration in $Ni_2Cu_1Sn_4$, which also weakens the binding between Ni and Sn. The Cu atoms cannot accommodate the loss of the binding between Ni and Sn, as the Cu *d* state peak position exactly corresponds to the saddle-point position of Sn *p* at the energy level of about −3.5 eV. Overall, the binding energy in the $Ni_2Cu_1Sn_4$ crystal structure is expected to be weaker than that of Ni_3Sn_4, which is consistent with the heat of formation results, as well as the polycrystalline stiffness results.

When the Cu solubility in $(Ni,Cu)_3Sn_4$ increases to 28.6 at.% (i.e., $Ni_1Cu_2Sn_4$), the amplitude of the Ni *d* state peak is further reduced, as shown in Fig. 6. In the meantime, the amplitude of the Sn *p* state at around −3.0 eV is also dramatically lowered. Similar to $Ni_2Cu_1Sn_4$, hybridization between Cu *d* and Sn *p* states is still not able to accommodate the loss of binding energy between Ni and Sn in $Ni_1Cu_2Sn_4$. Therefore, the binding energy in $Ni_1Cu_2Sn_4$ decreases as well, which is also in good agreement with the results on thermodynamic stability and elastic properties, as shown in Tables II and III.

To investigate the anisotropic elastic properties of Ni_3Sn_4 single crystal, an external normal strain of 10% was prescribed in different directions. According to Fig. 2a, c_{33} is the largest while c_{11} is the smallest in Ni_3Sn_4. Thus a tensile strain of 10% was applied in the *x*- and *z*-directions, respectively. We have demonstrated that hybridization between Ni *d* and Sn *p* states is the dominant factor of binding in Ni_3Sn_4. In addition, the Sn *p* state has nearly the same bandwidth as those of Ni *d* at the Fermi energy between 0 eV and −6 eV. Accordingly, the integrated total amount of Ni *d* state below the Fermi level was extracted to assess the change of the electronic states versus the applied strain. Figure 7 illustrates the integrated PDOS of Ni and

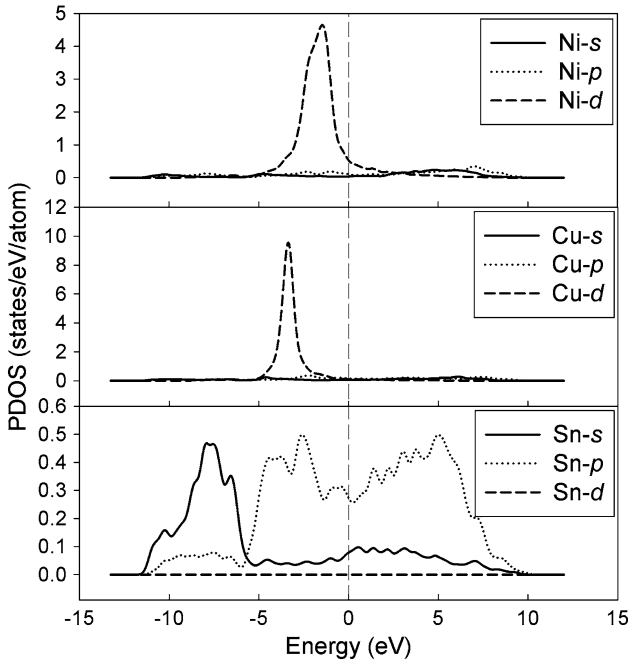

Fig. 5. PDOS of Ni, Cu, and Sn atoms in $Ni_2Cu_1Sn_4$.

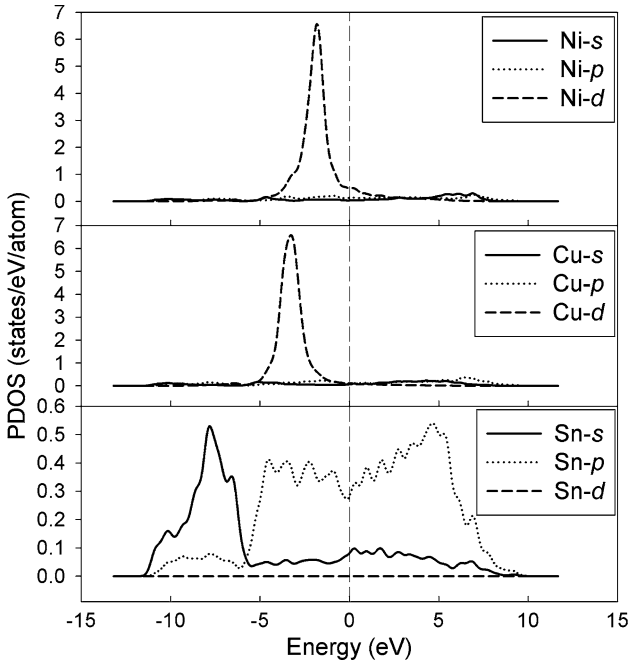

Fig. 6. PDOS of Ni, Cu, and Sn atoms in $Ni_1Cu_2Sn_4$.

Sn atoms below the Fermi level after the normal strain was applied in the x- and z-directions. It was found that, in comparison with the undeformed structure, the total amount of the Ni d state decreased by 0.004 under an external strain ε_{xx} = 0.1, and by 0.021 under an external strain ε_{zz} = 0.1. In the meantime, the total amount of the Sn p state decreased by 0.160 under an external strain ε_{xx} = 0.1,

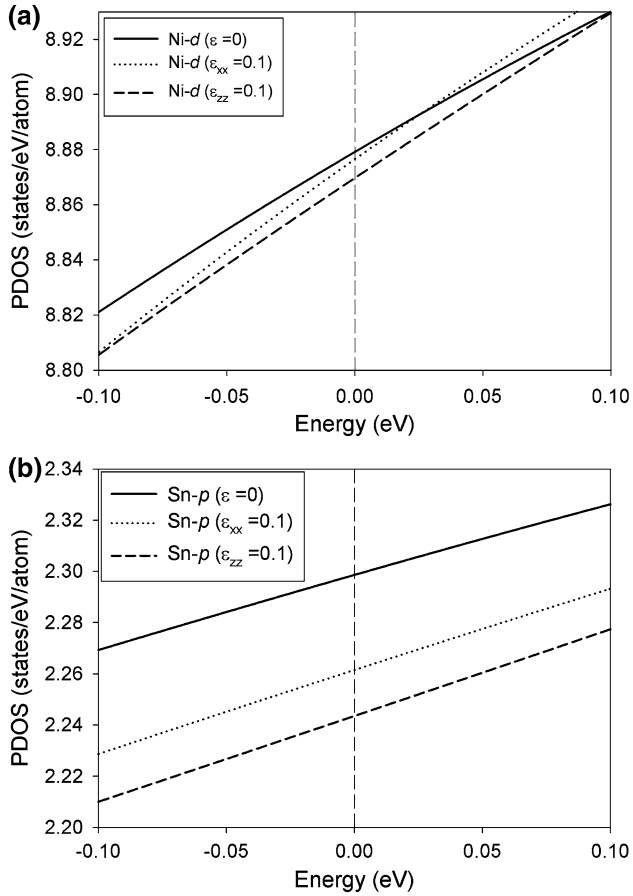

Fig. 7. Integrated PDOS of Ni states and Sn states under an external principle strain 0.1: (a) Ni d state change due to principle strain 0.1, and (b) Sn p state change due to principle strain 0.1.

and by 0.230 under an (forthcoming) external strain ε_{zz} = 0.1. Clearly, these results suggest that the changes of both Ni d and Sn p states versus ε_{zz} are larger than those versus ε_{xx}, revealing a larger stiffness against ε_{zz} than against ε_{xx}.

CONCLUSIONS

A first-principles approach was used to study the structure and elastic properties of $(Ni,Cu)_3Sn_4$-based IMCs. The following conclusions are drawn:

1. The thermodynamic stability of $(Ni,Cu)_3Sn_4$-based IMCs was investigated by calculating the heat of formation. It was found that the thermodynamic stability decreases with increasing Cu concentration, with Ni_3Sn_4 being the most stable composition. This indicates that Cu solubility in the $(Ni,Cu)_3Sn_4$ crystal structure is less than 14.3 at.%, consistent with existing experimental results.
2. The polycrystalline elastic properties of $(Ni,Cu)_3Sn_4$ were extracted based on the calculated single-crystal elastic constants. The Ni_3Sn_4 phase shows larger moduli than those of $Ni_2Cu_1Sn_4$ and $Ni_1Cu_2Sn_4$. The electronic structure

calculation results show that hybridization of Ni d and Sn p states governs binding in Ni_3Sn_4. The reduced moduli of $Ni_2Cu_1Sn_4$ and $Ni_1Cu_2Sn_4$ were attributed to decreased hybridization between Ni d and Sn p states.

3. The Ni_3Sn_4 phase exhibits anisotropic elastic properties. This is because the changes of the electronic states are different for strains applied in different directions. It is demonstrated that the changes of both Ni d and Sn p states in Ni_3Sn_4 are more pronounced for strain applied along the directions with larger stiffness.

ACKNOWLEDGEMENTS

The author F.G. is grateful to Dr. Lee and Dr. Tan, National University of Singapore for invaluable discussion.

REFERENCES

1. G. Ghosh, *J. Electron. Mater.* 33, 229 (2004).
2. C.-H. Lin, S.-W. Chen, and C.-H. Wang, *J. Electron. Mater.* 31, 907 (2002).
3. S.-W. Chen, S.-H. Wu, and S.-W. Lee, *J. Electron. Mater.* 32, 1188 (2003).
4. F. Gao, H. Nishikawa, and T. Takemoto, *J. Electron. Mater.* 37, 45 (2008).
5. Z. Chen, M. He, B. Balakrishnan, and C.C. Chum, *Mater. Sci. Eng. A* 423, 107 (2006).
6. G.-Y. Jang, J.-W. Lee, and J.-G. Duh, *J. Electron. Mater.* 33, 1103 (2004).
7. K. Mohankumar and A.A.O. Tay, *Proceedings of the 2004 Electronics Packaging Technology conference* (Piscataway, NJ, 2004), pp. 483–489.
8. H.J. Albrecht, A. Juritza, K. Muller, J. Sterthaus, J. Willian, and A. Vogliano, *Proceedings of the 2003 Electronics Packaging Technology conference* (Piscataway, NJ, 2003), pp. 726–731.
9. G. Ghosh, *J. Mater. Res.* 19, 1439 (2004).
10. N.T.S. Lee, V.B.C. Tan, and K.M. Lim, *Appl. Phys. Lett.* 88, 031913-1 (2006).
11. N.T.S. Lee, V.B.C. Tan, and K.M. Lim, *Appl. Phys. Lett.* 89, 131908-1 (2006).
12. J. Chen, Y.-S. Lai, C.-Y. Ren, and D.-J. Huang, *Appl. Phys. Lett.* 92, 081901 (2008).
13. W. Jeitschko and B. Jaberg, *Acta Crystallogr.* B38, 598 (1982).
14. S.J. Clark, M.D. Segall, C.J. Pickard, P.J. Hasnip, M.J. Probert, K. Refson, and M.C. Payne, *Z. Kristallogr.* 220, 567 (2005).
15. Materials Studio version 4.4 (San Diego, CA: Accelrys, 2008).
16. B.B. Karki, L. Stixrude, S.J. Clark, M.C. Warren, G.J. Ackland, and J. Crain, *Am. Mineral.* 82, 635 (1997).
17. A. Gangulee, G.C. Das, and M.B. Bever, *Metall. Trans.* 4, 2063 (1973).
18. G. Ghosh, *Metall. Mater. Trans.* 40A, 4 (2009).
19. P. Nash, H. Choo, and R.B. Schwarz, *J. Mater. Sci.* 33, 4929 (1998).
20. G. Ghosh, *Metall. Mater. Trans.* 30A, 1481 (1999).
21. H.D. Dannohl and H.L. Lukas, *Z. Metallkd.* 65, 642 (1974).
22. A.N. Torgersen, H. Bros, R. Castanet, and A. Kjekhus, *J. Alloys Compd.* 307, 167 (2000).
23. W.T. Chen, C.E. Ho, and C.R. Kao, *J. Mater. Res.* 17, 263 (2002).
24. R. Hill, *Proc. Phys. Soc. Lond. Sec. A* 65, 349 (1952).
25. L.H. Xu and J.H.L. Pang, *Thin Solid Films* 504, 362 (2006).